HHS Public Access

Author manuscript

Inhal Toxicol. Author manuscript; available in PMC 2023 August 22.

Published in final edited form as:

Inhal Toxicol. 2021 February ; 33(2): 66–80. doi:10.1080/08958378.2021.1884320.

Lung toxicity and gene expression changes in response to whole-body inhalation exposure to cellulose nanocrystal in rats

Pius Joseph,

Christina M. Umbright,

Jenny R. Roberts,

Jared L. Cumpston,

Marlene S. Orandle,

Walter G. McKinney,

Tina M. Sager

Health Effects Laboratory Division, National Institute for Occupational Safety and Health, Morgantown, WV, USA

Abstract

Objective: Human exposure to cellulose nanocrystal (CNC) is possible during the production and/or use of products containing CNC. The objectives of the current study were to determine the lung toxicity of CNC and the underlying molecular mechanisms of the toxicity.

Methods: Rats were exposed to air or CNC (20 mg/m^3, six hours/day, 14 d) by whole-body inhalation and lung toxicity and global gene expression profile were determined.

Results: Significant increases in lactate dehydrogenase activity, pro-inflammatory cytokine levels, phagocyte oxidant production, and macrophage and neutrophil counts were detected in the bronchoalveolar lavage cells or fluid from the CNC exposed rats. Mild lung histological changes, such as the accumulation of macrophages and neutrophils, were detected in the CNC exposed rats. Gene expression profiling by next generation sequencing identified 531 genes whose expressions were significantly different in the lungs of the CNC exposed rats, compared with the controls. Bioinformatic analysis of the lung gene expression data identified significant enrichment in several biological functions and canonical pathways including those related to inflammation (cellular movement, immune cell trafficking, inflammatory diseases and response, respiratory disease,

CONTACT Pius Joseph pcj5@cdc.gov Toxicology and Molecular Biology Branch, National Institute for Occupational Safety and Health, 1095 Willowdale Road, Morgantown, WV 26505, USA.

The Next Generation Sequence data discussed in this publication have been deposited in NCBI's Gene Expression Omnibus (GEO) and are accessible through GEO Series accession number GSE150567.

Supplemental data for this article can be accessed at https://doi.org/10.1080/08958378.2021.1884320.

Disclosure statement

The authors declare no potential conflicts of interest with respect to the research, authorship, and/or publication of this article.

Disclaimer

The findings and conclusions in this report are those of the authors and do not necessarily represent the official position of the National Institute for Occupational Safety and Health, Centers for Disease Control and Prevention.

complement system, acute phase response, leukocyte extravasation signaling, granulocyte and agranulocyte adhesion and diapedesis, IL-10 signaling, and phagosome formation and maturation) and oxidative stress (NRF2-mediated oxidative stress response, production of nitric oxide and reactive oxygen species in macrophages, and free radical scavenging).

Conclusion: Our data demonstrated that inhalation exposure of rats to CNC resulted in lung toxicity mediated mainly through the induction of inflammation and oxidative stress.

Keywords

Cellulose nanocrystal (CNC); lung toxicity; rat; mechanisms; gene expression; inflammation; oxidative stress

Introduction

Cellulose, the most abundant organic polymer in the biosphere, is formed by hydrogen bonding between adjacent glucose monomers and is a major component of plants, bacteria, fungi, and tunicates (Siro and Plackett 2010). Cellulose, widely considered as nontoxic, has numerous applications. It is a major component of the food cycle. Cellulose insulation, manufactured by the shredding and milling of old newspapers and the addition of fire retardant(s), is widely used as a type of thermal insulation in the construction industry (Morgan 2006). Aerosolization of respirable cellulose particles, during the manufacture and use of cellulose insulation is possible resulting in exposure of workers to the particles. This prompted the US National Toxicology Program (NTP) to conduct a study regarding the toxicity potential and health effects of cellulose. Based on the results of human studies, the NTP has concluded that inhalation exposure to the cellulose particles generated from cellulose insulation resulted in only minimal pulmonary toxicity which is attributed mainly to the chemical elements present in the fire retardant(s) added during manufacturing the cellulose insulation (Morgan 2006). Currently, the Occupational Safety and Health Administration (OSHA) regulates exposure to cellulose at a permissible exposure limit (PEL) of 15 mg/m^3 (total particulate) and 5 mg/m^3 (respirable particulate) (NIOSH 2019).

A reduction in size of materials facilitates the generation of nanomaterials (<100 nm at least in one dimension) with many unique and desirable physical and chemical properties. Nanocellulose can be generated from large sized cellulose fibers either by physical or chemical processing. Acid hydrolysis of cellulose results in the generation of cellulose nanocrystal (CNC) while mechanical processing, for example shearing of cellulose by homogenization, results in the generation of cellulose nanofibril (CNF) (Charreau et al. 2013). The whisker-shaped CNC is characterized by a high degree of crystallinity (~54–88%) and high aspect ratio (Moon et al. 2011). The many desirable physical properties of CNC, viz. high tensile strength and rigidity, high aspect ratio and surface area, low density, liquid crystalline behavior, high water absorption capacity, thermal stability, and ability to be easily obtained by chemical modifications (Habibi et al. 2010; Rol et al. 2020) offer many valuable applications as composites (Lee et al. 2012), in electronic products (Hubbe et al. 2008), in biomedical engineering (Mathew et al. 2013), and in drug delivery (Seabra et al. 2018). Additionally, CNC is inexpensive, biodegradable, biocompatible, and sustainable.

Despite the numerous applications of nanomaterials like CNC, mainly due to their many highly desirable physical and chemical properties, they may present unique challenges and significant concern with respect to human safety and health. Due to their small size, CNC and other nanomaterials are easily aerosolized and the air-born nanoparticles, following inhalation, may be deposited deep in the lungs to result in toxicity. The toxicokinetics of nanomaterials such as absorption, distribution, metabolism, and elimination may be considerably different compared with the parent, large sized particles. These can potentially result in either novel toxicity or alteration in severity of toxicity exerted by the nanomaterial compared with the large-sized parent material. In the past, few studies have been conducted investigating the toxicity potential of CNC. The lung bio-durability of CNC and its ability to generate hydroxyl radical, a toxic reactive oxygen species (ROS), in a cell-free system was significantly higher compared with micron-sized cellulose particles (Stefaniak et al. 2014). In an *in vitro* study conducted by Endes et al. (2014), a 3D human airway multi-cellular barrier model was exposed to CNC extracted by acid hydrolysis from paper and tunicates at concentrations ranging from 0.14 to 1.57 μg/cm^2. No significant cytotoxicity, oxidative stress, or proinflammatory responses were reported up to the highest concentration of the CNC employed. Menas et al. (2017) compared the toxicity of CNC and CNF particles in human lung epithelial A549 cells. The CNF particles resulted in higher cytotoxicity and oxidative damage whereas the CNC particles resulted in a more robust inflammatory response in the A549 cells. *In vitro* exposure of non-cancerous human bronchial epithelial cells, BEAS-2B, to CNC resulted in DNA damage and cellular neoplastic transformation characteristics such as increased proliferation, colony formation, anchorage-independent growth, and cell migration and invasion (Kisin et al. 2020). In a C57BL/6 mouse study, Yanamala et al. (2014) administered two physical forms of CNC - a suspension and a powder, by pharyngeal aspiration and the resulting pulmonary toxicity was compared with that induced by asbestos. Overall, on a mass basis, the quantitative differences in the toxicity parameters assessed were more significant in the mice administered both the CNC particles compared to those administered asbestos. Between the two groups, the responses were more pronounced in the CNC gel suspension compared with the CNC powder suspended in water and administered by pharyngeal aspiration to mice. Based on these results, the authors concluded that the CNC particles are more toxic than asbestos and the suspension form of CNC is more toxic than the powder form. In a subsequent study (Shvedova et al. 2016), the lung toxicity following pharyngeal aspiration of the CNC powder form was investigated in male and female C57BL/6 mice. A more pronounced lung toxicity, in response to the CNC exposure, was detected in the female mice compared to their male counterparts implying that the CNC-induced lung toxicity in mice is gender-dependent (Shvedova et al. 2016; Shatkin and Oberdorster 2016). It has also been reported that pharyngeal aspiration of CNC in mice modulated their immune system (Park et al. 2018) and resulted in deleterious effects in the male reproductive system (Farcas et al. 2016).

In the current study, the lung toxicity potential of CNC in response to whole-body inhalation exposure in rats was investigated and the molecular mechanisms underlying the toxicity was determined. To the best of our knowledge, this is the first study in which rats were exposed to CNC by inhalation, the most likely route for occupational exposure to CNC, to investigate the lung toxicity potential and the underlying molecular mechanisms.

Materials and methods

Animals

The entire animal study was conducted in an AAALAC International accredited animal facility (NIOSH, Morgantown, WV) following a protocol approved by the CDC-Morgantown Institutional Animal Care and Use Committee. Approximately 3 months old, healthy, male Fischer 344 rats (CDF strain) purchased from Charles River Laboratories (Wilmington, MA) were used in this study. Throughout the entire period of the study, the rats were housed in groups of 3 rats/cage and maintained on a 12h light-dark cycle in a temperature (68–72 °F) and humidity (30–70%) controlled room. The rats were provided with Teklad rodent diet (Envigo, Indianapolis, IN) and tap water *ad libitum* except when they were exposed to air or CNC as described below.

Cellulose nanocrystal

CNC obtained from the Forest Products Laboratory, United States Forest Services (Madison, WI), without any further processing or purification, was used in this study. Details regarding the physical and chemical characterization of the CNC sample have been reported by investigators from our institute who have used the same material in their studies (Stefaniak et al. 2014; Yanamala et al. 2014; Shvedova et al. 2016).

Generation and characterization of CNC aerosol

An aerosol for inhalation exposure was generated from a bulk supply of CNC. An automated, computer-controlled system was used to generate and deliver precise concentrations of dispersed airborne CNC particles to the inhalation exposure chamber containing the rats. The design of the aerosol generation and exposure system was based on a previously developed system (McKinney et al. 2013). In brief, a custom-built acoustical generator with a venturi stage was used to generate an aerosol containing CNC particles. The aerosol generation and exposure system, combined air flow controllers, aerosol particle monitors, data acquisition devices, and custom software with automatic feedback control to achieve constant and repeatable chamber temperature, relative humidity, pressure, aerosol concentration, and particle size distribution.

Aerodynamic particle mass size distribution of the CNC aerosol generated for the rat exposure was determined using a micro-orifice uniform deposit impactor (MOUDI Model 110 R, MSP Corporation, Shoreview, MN). Greased foils were used for the MOUDI stages. The mass distribution for the CNC particles within the exposure chamber is presented in Figure 1(A). MOUDI readings were taken with fresh CNC powder and after six hours of use inside the particle generator. There was no significant difference between the two readings. Mass size distribution was also measured at two chamber concentration levels (5 mg/m^3 and 20 mg/m^3), and again there was no significant difference between the two measurements. The MOUDI data showed a bimodal mass size distribution with mass median aerodynamic diameters of 140 nm, and 2.5 μm (Figure 1(A)). The particle sizes spanned from 50 nm to 15 μm.

A scanning electron microscope (Hitachi S-4800) was used to analyze particle physical morphology by drawing aerosol samples at a flow rate of 1 L/min from the sample chamber onto 25 mm (0.2 μm pore size) polycarbonate filters (Whatman, Inc., Maidstone, United Kingdom) for approximately 5 s. Figure 1(B) shows examples of CNC particles on the filters. Unlike the freeze-dried CNC sample which consisted of large compact aggregates (Beck et al. 2012), the physical sizes of the uniformly distributed CNC particles generated in the aerosol ranged from 100 nm diameter up to over 10 μm diameters. The shapes and sizes of the particles also varied: some were fiber like, sheet like, small and spherical, or large chunks with jagged edges (Figure 1(B)).

Inhalation exposure of rats to CNC aerosol

Two groups of rats (n=12), following an acclimatization period to the animal facility conditions of at least 10 days, were exposed simultaneously by whole-body inhalation to air (control) or CNC aerosol. The concentration of CNC particles in the aerosol was maintained at a target level of 20 mg/m^3, six hours/day, five consecutive days/week for 14 days (Monday to Friday during the first two weeks and Monday to Thursday during the third week). The CNC concentration employed in the study was selected based on the results of a preliminary study (20 mg/m^3, six hours/day, four days) that did not result in any detectable lung toxicity in the rats. The selected concentration was approximately three times the OSHA PEL and National Institute for Occupational Safety and Health (NIOSH) recommended exposure limit (REL) for respirable size cellulose (NIOSH 2019). Since, currently, there is no REL or PEL established for CNC, the dose selected in this study was based on those for respirable size cellulose. In addition, due to the very low mass of CNC particles, it was impossible to generate higher concentrations of CNC aerosol to conduct a dose-response study. The animals were not provided with food and water while they were in the exposure chamber for the whole-body inhalation exposure. Sixteen hours following termination of the last exposure to air or CNC aerosol, the rats were euthanized, and lung toxicity and gene expression profile determined as described in the following sections.

Euthanasia of rats and collection of biospecimens

For euthanasia, the rats were given an intraperitoneal injection of pentobarbital euthanasia solution (Fort Dodge Animal Health, Fort Dodge, IA). Blood was collected, under anesthesia, directly from the abdominal aorta into Vacutainer tubes (Becton-Dickinson, Franklin Lakes, NJ) containing EDTA and mixed well. Bronchoalveolar lavage (BAL) was performed in the left lung lobes as previously described (Roberts et al. 2014). The BAL samples collected were centrifuged (500xg, 10 min, 4 °C) to separate the cellular and acellular fractions. The cell pellet obtained was resuspended in 1 ml PBS buffer and used along with the BAL fluid for assessment of lung toxicity as described in the corresponding sections below. The diaphragmatic and cardiac lobes of the unlavaged right lung were inflated with 10% neutral buffered formaldehyde and stored in the same solution until used for histopathological analysis. The unlavaged right apical lung lobe was cut into small pieces, stored in RNALater (Invitrogen, Carlsbad, CA), and used to determine gene expression profile.

Hematology

Various hematological parameters were determined in the unclotted blood samples using an IDEXX Procyte instrument (IDEXX Corporation, Westbrook, ME) following the procedures described in the user guide. The hematological parameters analyzed included counts of white blood cells (WBCs), red blood cells (RBCs), neutrophils (NEUTs), lymphocytes (LMPHs), monocytes (MONOs), eosinophils (EOs), basophils (BASOs), platelets (PLT), and reticulocytes (RET), red blood cell distribution (RDW), hemoglobin (HGB), hematocrit (HCT), mean corpuscular volume (MCV), mean corpuscular hemoglobin (MCH), platelet distribution width (PDW), mean platelet volume (MPV), and platelet larger cell ratio (P-LCR).

Lung histopathology

The fomaldehyde fixed lung lobes were paraffin embedded, sectioned at a thickness of 5 μm, stained with hematoxylin and eosin (H&E) and examined by a pathologist using bright field and polarizing light microscopy (for visualizing particles/crystals). The severity of non-neoplastic lung lesions was graded using a 4-point scoring system (0=Within normal limits. The tissue is considered to be normal; 1= Minimal. This corresponds to a histologic change that is barely noticeable; 2=Mild. This corresponds to a histologic change that is noticeable but is not a prominent feature of the tissue; 3=Moderate. This corresponds to a change that is a prominent feature of the tissue; and 4=Severe. This corresponds to a change that is an overwhelming feature of the tissue) (Shackelford et al. 2002; Mann et al. 2012).

Lactate dehydrogenase activity

Lactate dehydrogenase (LDH) activity, a general indicator of cytotoxicity (Ameen et al. 2003), in the acellular BAL fluid (BALF) was determined with a COBAS C111 analyzer (Roche Diagnostic Systems, Mountclair, NJ) as previously described (Sellamuthu et al. 2011).

BAL cell counts

The total number of cells present in the BAL cellular fraction prepared was determined using a Coulter Multisizer II and Accu Comp software (Coulter Electronics, Hialeah, FL). BAL cells (5×10^4) were spun onto microscope slides using a Cytospin 3 centrifuge (Shandon Life Sciences International, Cheshire, England) and stained with a Leukostat stain (Fisher Scientific, Pittsburgh, PA) to differentiate alveolar macrophages (AM) and PMN. At least 200 cells were counted per BAL sample and percentages were multiplied back across the total cell count to obtain total number of AM, PMN, and any other cells present in the sample. The number of multinucleated AMs present in a sub-set of BAL samples (n=6) was also recorded. CNC particles engulfed by the BAL cells were detected by examining the cytospin slides using a polarizing light microscope.

BALF cytokines

The BALF levels of 6 inflammatory cytokines (IL-1β, IL-10, IL-12, MCP-1, MIP-2, and TNF-α) were determined using a multiplexing ELISA kit (Millipore Corporation, Billerica, MA) and a Luminex MAGPIX® reader (Luminex Corporation, Austin, TX). The ELISA

data was acquired with Luminex Xponent software and analyzed with MILLIPLEX Analyst 5.1 (EMD Millipore Corporation, Billerica, MA).

Reactive oxygen species (ROS) generation by BAL cells

The generation of ROS by the phagocytes, AM and PMN, present in the BAL was determined by a luminol-dependent chemiluminescence assay (Roberts et al. 2014). The contribution of AM and PMN in the production of ROS was determined using the stimulants, phorbol 12-myristate 13-acetate (PMA) – stimulant of AM and PMN, and non-opsonized, insoluble zymosan – a stimulant of AM only. A resuspension of the BAL cells, equivalent to 5×10^5 total BAL cells or 5×10^5AM, was incubated with the luminol for 10 min at 37 °C which was followed by stimulation of the cells with either 10 μM PMA or 1 μg zymosan, respectively, in a total volume of 500 ml. The oxidant production by the BAL cells in the absence of the stimulants was measured and considered as the baseline. A Berthold LB 953 luminometer (Wildbad, Germany) was used for the measurement of CL for 15 min at 37° C, and the integral of counts per minute (cpm) per one million cells versus time was calculated. The cpm of the stimulated cells minus the cpm of the corresponding resting cells was calculated and the value was normalized to the total number of BAL cells for PMA-stimulated CL and total number of AM for zymosan-stimulated CL.

Lung gene expression profile

Total RNA, free of contaminating proteins and DNA, was isolated from a piece of the lung tissue stored in RNALater using a miRNeasy Mini Kit (Qiagen, Inc. Valencia, CA). The procedure, including the on-column DNase digestion, provided by the manufacturer was followed for RNA isolation. The RNA samples were analyzed for their integrity and purity using an Agilent 2100 Bioanalyzer and RNA 6000 Nano Kit (Agilent Technologies, Palo Alto, CA) and quantified by UV-Vis spectrophotometry. Undegraded RNA samples with an RNA Integrity Number (RIN) >8.5 were used in the gene expression studies.

One microgram total RNA/sample was used to create sequencing libraries using the Illumina TruSeq® Stranded mRNA Library Prep Kit (Illumina, Inc. San Diego, CA) following the protocol provided by the manufacturer. Stated briefly, the poly-A containing mRNA molecules were isolated using poly-T oligo attached magnetic beads to remove ribosomal RNA and any other non-mRNA. The purified mRNA samples were fragmented (68 °C for 5 min) and reverse transcribed into first strand cDNA using reverse transcriptase and random primers. While synthesizing the double stranded cDNA, dUTP was incorporated in place of dTTP followed by the addition of a single ‘A’ nucleotide to the 3 prime ends to ligate the indexing adapters provided in the library preparation kit. The samples were PCR amplified (12 cycles) to enrich the DNA fragments containing the adapter molecules in the library using a Veriti™ 96 Well Thermal Cycler (Applied Biosystems, Foster City, CA). The PCR amplified cDNA library samples were quantified using a dsDNA HS Assay Kit (Invitrogen by ThermoFisher Scientific, Waltham, MA) and Qubit 3.0 Fluorometer (Invitrogen by ThermoFisher Scientific, Waltham, MA). Average fragment size and fragment distribution of the cDNA library samples were then assessed using an Agilent 2100 Bioanalyzer with High Sensitivity DNA Reagents (Agilent Technologies, Santa Clara, CA).

Individual sample libraries were provided to the Centers for Disease Control and Prevention Genome Sequencing Laboratory (GSL; Atlanta, GA) for 2×75 base pair, paired- end sequencing using the Illumina Hiseq 2500 (Illumina, San Diego, CA) in rapid run mode using HiSeq Rapid Cluster Kit v2 (Illumina, San Diego, CA) and HiSeq Rapid SBS Kit v2 (Illumina, San Diego, CA). After the library sequences were demultiplexed by the GSL, the quality of each sample library was assessed with respect to the number of reads per sample, mean quality score, and FASTQC parameters (Andrews 2010). Reads were then processed using Trimmomatic/0.35 with the options PE, ILLUMINACLIP:TruSeq2-PE.fa:2:30:10 LEADING:3 TRAILING:3 SLIDINGWINDOW:4:15 MINLEN:60 to remove any remaining adapter sequence, low quality reads, low quality read ends, and sequences shorter than 60 bases in length (Bolger et al. 2014). Sequence quality was then reevaluated via FASTQC. All sequences that passed the trimming and quality control with both reads in a pair present were aligned to the *Rattus norvegicus* Rnor 6.0 genome from NCBI downloaded July 31st, 2015 using HiSat2/2.1.0 (Kim et al. 2015). Raw gene counts were assigned using Samtools/1.8 (Li et al. 2009), Python/2.7.3 and HTSeq/1.11.2. Using edgeR, raw counts were converted to counts per million (CPM), log-CPM, and normalized using the trimmed mean of M-values (TMM) method. Finally, differentially expressed genes were calculated using limma (Law et al. 2016; R Core Team 2018). Significantly differentially expressed genes (SDEGs) were those genes with an absolute fold change greater than 1.5-fold and an adjusted p-value less than 0.05.

Bioinformatic analysis of differentially expressed genes

Bioinformatic analysis of the SDEGs was performed using Ingenuity Pathway Analysis (IPA) (Qiagen, Inc, Valencia, CA) and Gene Ontology (GO) enrichment analysis (http://geneontology.org/) programs. These programs map the biological relationship of the input genes and classify them into categories such as biological functions and processes, canonical pathways, diseases, and networks.

Statistical analysis of data

All data except for NGS data between the exposed and control groups were compared using Student's t-tests. The level of statistical significance was set at $p < 0.05$.

Results

Clinical signs of toxicity in the rats

Except for a 5.7% reduction ($p < 0.05$) in body weight by the end of the study (Figure 2), no other clinical sign of toxicity was detected in the CNC exposed rats, compared with the controls.

Lung deposition of CNC particles

Exposure of rats to CNC resulted in lung deposition of the inhaled particles as evidenced by the detection of birefringent CNC particles in the lung sections under polarizing light (Figure 3(A,B)). Furthermore, the inhaled CNC particles were mostly found engulfed by the AMs (Figure 4(A,B)). The animal exposure of CNC to 20 mg/m^3, 6 hrs/day for 14 days will result in an alveolar deposited dose of 1.190 mg based on the MPPD model

(Anjilvel and Asgharian 1995). This dose can be scaled to a human equivalent dose by using known alveolar surface area values of 70 m^2 and 0.4 m^2, respectively, for human and rat lungs (Butler 1976; Ohashi et al. 1994). By using these values, the equivalent human alveolar lung burden resulting from the CNC exposure was estimated and found to be 208 mg. Assuming that the deposition efficiency of the particles is 14% in the human pulmonary region, based on the MPPD model, the rat exposure conducted in this study will be equivalent to an average worker's exposure for approximately 8.25 weeks at the PEL of 5 mg/m^3 for respirable size cellulose (NIOSH 2019). Both the alveolar deposition and the human equivalence of CNC estimated in our rat study were comparable to those reported by Shvedova et al. (2016) in their mouse study.

Lung histopathology

Lungs from 10 of the 12 control animals were essentially normal, 2 controls had focal areas of inflammation or accumulations of alveolar macrophages. All animals exposed to CNC had diffuse, minimal to mild accumulation of alveolar macrophages (alveolar histiocytosis) sometimes accompanied by small foci of alveolar inflammation/alveolitis (4/12 animals). Alveolar inflammation in these animals was minimal and consisted of small numbers of macrophages and neutrophils (Figure 3(C,D)). No other histological change indicative of pathology was detected in the airways, alveoli, or blood vessels of the CNC exposed rats. The alveolar histiocytosis scores in the air and CNC exposed rats were 0.17 ± 0.17 and 1.58 ± 0.15, respectively. Similarly, alveolitis scores in the control and CNC exposed rats were 0.083 ± 0.08 and 0.42 ± 0.15, respectively. Particle-laden macrophages were often seen using polarizing light microscopy (birefringent crystals). These macrophages were typically randomly distributed, or less frequently located at terminal bronchioles or alveolar ducts (Figure 3(A,B)).

BAL parameters of toxicity

Results obtained from the various BAL parameters of toxicity evaluated in the rats indicated lung toxicity induction in the CNC exposed rats, compared with those exposed to air alone. Lactate dehydrogenase activity was significantly ($p<0.05$) elevated in response to CNC exposure in the rat lungs (Figure 5(A)). Similarly, the number of total BAL cells, AM, and PMN in the lungs of the CNC exposed rats was significantly ($p<0.05$) higher than those in the control group of rats (Figure 5(B–D)). The number of total BAL cells and AMs increased by 21.4% and 13.5%, respectively, in the CNC exposed rat lungs compared with those in the controls. The number of PMNs, on the other hand, showed a much higher 22.7-fold, increase in the CNC exposed rat lungs, compared with the control lungs. However, the increase in PMN in the rats was lower than the 31-fold increase reported by Shvedova et al. (2016) in the male mouse exposed to CNC by pharyngeal aspiration. A statistically significant ($p<0.05$) increase (2.68-fold) in the number of binucleated AMs was also detected in the CNC exposed rat lungs compared with the controls (Figures 4(C,D) and Figure 6).

Oxidant generation in rat lungs

The PMA and zymosan-stimulated oxidant generation by the phagocytes obtained from the CNC exposed rat lungs showed a statistically significant (p<0.05) increase of 13.11- and 2.95-fold, respectively, compared with those obtained from the control rat lungs (Figure 7).

Induction of inflammation in rat lungs

A statistically significant increase in three out of the six cytokines analyzed was detected in the BALF obtained from the CNC exposed rat lungs compared with the controls (Figure 8). The BALF level of MIP-2 was 89% higher in the CNC exposed rat lungs compared with the controls while those of MCP-1 and TNF-α were 41% and 20%, higher, respectively. The increase in the BALF MCP-1 in the CNC exposed rats was lower compared to the 2.35-fold increase reported by Shvedova et al. (2016) in the male mouse exposed to CNC by pharyngeal aspiration.

Hematology

Mild, but statistically significant differences (p>0.05), between the control and CNC exposed groups of rats were noticed in six out of the 26 hematological parameters analyzed (Table 1). The number of red blood cells (RBCs) and the percentage of neutrophils among the white blood cells were higher in the CNC exposed rats compared with the controls. On the other hand, RDW-SD, RET, P-LCR were significantly lower in the blood of the rats in response to CNC exposure.

Lung gene expression profile

Any gene that exhibited a > 1.5-fold change in the expression and an adjusted p value <0.05 for the change between the CNC exposed and control groups of rat lungs was considered an SDEG. Using this selection criteria, the expressions of 531 genes were found to be significantly different between the CNC exposed and the air exposed groups of rats (a list of the SDEGs with fold changes in their expressions and the adjusted p values is presented in Supplemental Table 1). Among the 531 SDEGs, the expression of 424 and 107 transcripts were up- and down-regulated, respectively, in response to the CNC exposure. The SDEG with the highest overexpression was *Defensin b5 (DEFb5)* (17.21-fold change) while among the down-regulated SDEGs, *Delta like non-canonical notch ligand 1 (DLK1)* ranked first (−20.03-fold change) (Tables 2 and 3). The changes in gene expressions in response to CNC exposure was confirmed by the results of real time PCR analysis (data not presented).

Bioinformatic analysis of the SDEGs detected in the CNC exposed rat lungs identified significant enrichment in multiple IPA diseases and biological function categories. The top 10 most significantly enriched IPA diseases and biological function categories were transport of molecules, quantity of cells, inflammation of organ, rheumatic disease, inflammation of absolute anatomical region, cell movement of blood cells, leukocyte migration, inflammatory response, cell movement of leukocytes, and recruitment of granulocytes (Figure 9). Many other IPA biological functions related to cancer, oxidative stress, and fibrosis were also significantly enriched in response to CNC exposure (Supplemental Table 2). The top 10 most significantly enriched IPA canonical pathways were acute phase response signaling, granulocyte adhesion and diapedesis, agranulocyte

adhesion and diapedesis, LXR/RXR activation, FXR/RXR activation, altered T cell and B cell signaling in rheumatoid arthritis, communication between innate and adaptive immune cells, phagosome formation, complement system, and role of IL-17A in psoriasis (Figure 10). Other significantly enriched canonical pathways included GADD45 signaling, circadian rhythm signaling, role of pattern recognition receptors in recognition of bacteria and viruses, production of nitric oxide and ROS in macrophages, NRF2-mediated oxidative stress response, toll-like receptor signaling, NFκB signaling, PPAR signaling, IGF-1 signaling, HIF1α signaling, calcium signaling, mTOR signaling and many cancer-related pathways (Supplemental Table 3). Gene Ontology (GO) enrichment analysis of the SDEGs confirmed the significant enrichment in many of the functions and pathways detected by the IPA analysis (data not presented).

Discussion

Human exposure to toxic materials takes place under a variety of occupational settings. Inhalation of air containing toxic materials is a major mechanism for entry of toxic agents with significant health consequences among workers. Nanomaterials can be easily aerosolized resulting in a significant risk for inhalation exposure in humans. The inhaled nanoparticles are deposited in the lungs, including the alveoli, and may result in pulmonary toxicity (Bakand et al. 2012). Additionally, primarily due to their very small size, rigidity, and ability to penetrate membranes, nanoparticles may easily cross the lung epithelium to enter the circulation leading to their distribution to distant organs and exert systemic toxicity (Husain et al. 2015).

Cellulose, the most abundant polymer present in the biosphere has multiple uses. Manufacturing and use of products containing cellulose for various industrial and commercial purposes may result in the generation of aerosolized particles posing a significant threat for human exposure to cellulose by inhalation. However, it is known that respirable cellulose particles of larger sizes (>100 nm at least in one dimension) present little or no health risk to humans (Cullen et al. 2000; Morgan 2006; Clift et al. 2011). It has been demonstrated that the toxicity of materials is dependent on their sizes; many nontoxic materials exert toxicity when their particle size is reduced to the nano scale, i.e. less than 100 nm at least in one dimension (Papageorgiou et al. 2007; Mroz et al. 2008). Consistent with this observation, exposure to nano-sized cellulose particles resulted in toxicity in *in vitro* cell culture (Menas et al. 2017; Kisin et al. 2020) and *in vivo* animal (Yanamala et al. 2014; Farcas et al. 2016; Shvedova et al. 2016; Park et al. 2018) models of toxicity. Considering the importance of lungs, both as a route for occupational exposure to nanosized cellulose particles and the resulting toxicity, CNC-induced pulmonary toxicity has been the focus of investigation in many of the toxicity studies involving CNC. In all the animal pulmonary toxicity studies conducted to date, CNC administration was done by oropharyngeal aspiration (Yanamala et al. 2014; Farcas et al. 2016; Shvedova et al. 2016; Park et al. 2018). Recently, the literature on CNC-induced pulmonary toxicity was reviewed by Ede et al. (2019) and Sai and Fujita (2020) and emphasized the need to conduct studies aimed to investigate lung toxicity following whole-body inhalation exposure, the most relevant method for human exposure to CNC. To date, there is no study in the peer-reviewed

literature reporting the toxicity of CNC following inhalation (whole-body or nose-only) exposure to CNC.

The results of the current study in which rats were exposed by whole-body inhalation to air or an aerosol containing aggregated CNC demonstrated the lung toxicity potential of CNC. The detection of birefringent CNC particles in the lungs (Figure 3), mostly associated with AMs (Figure 4), indicated the lung deposition of inhaled CNC particles in the rats. As a mode of pulmonary particle clearance, the inhaled toxic particles are phagocytosed, by AMs for their elimination protecting the lungs and other potential target organs from the toxicity. However, the deposited particles, in the absence of efficient elimination, become available to interact with the lung epithelium and the cells present in the alveoli potentially resulting in pulmonary and systemic toxicity. The mild, but statistically significant, reduction in the body weights of the CNC exposed rats, compared with the controls (Figure 2), suggested that CNC exposure adversely affected the health of the rats. The significant increase in LDH activity (Figure 5(A)), a cytotoxicity marker (Ameen et al. 2003), in the BALF of the exposed rats suggested that CNC exposure resulted in lung toxicity in the rats. Further evidence for CNC-induced lung toxicity included lung histological changes (Figure 3), an increase in the number of BAL cells (Figure 5(B–D)) and binucleated AMs (Figure 6), enhanced oxidant generation (Figure 7), an increase in the BALF levels of inflammatory cytokines (Figure 8), and alteration in the global gene expression profile (Tables 2 and 3 and Supplemental Table 1) in the CNC exposed rats compared with the controls. Collectively, these data, as expected and in agreement with the results of previous animal studies (Yanamala et al. 2014; Shvedova et al. 2016; Farcas et al. 2016; Park et al. 2018), suggested that the whole-body inhalation exposure to CNC, under the conditions employed in our study, resulted in lung toxicity in the rats. Our findings that rats, similar to mouse, also exhibited lung toxicity in response to CNC exposure suggested that the CNC-induced lung toxicity is not species-specific and rats, a commonly employed animal model in toxicity studies, is also useful in determining the lung toxicity of CNC. However, whether the lung response to CNC exposure exhibit any gender difference in rats, like that reported in mouse (Shvedova et al. 2016), needs to be determined. Similarly, the hematological changes detected in the exposed rats (Table 1) may suggest the potential for CNC to result in systemic toxicity, especially under chronic exposure conditions, and needs further investigation.

Inhaled toxic particles in the lungs interact with phagocytes, primarily resident macrophages, and this may result in cytotoxicity and death of the macrophages. One of the consequences of particle-induced cytotoxicity and death of AMs is the release of reactive intermediates including those involved in an inflammatory response (Greenberg et al. 2007). The inflammatory intermediates released may function as signaling molecules to recruit additional phagocytes to the site of lung injury. A significant increase in the number of BAL cells, including AMs and PMNs, in the CNC exposed rat lungs compared with the air exposed controls (Figure 5(B–D)), suggested the recruitment of additional phagocytes, as part of an inflammatory response to the CNC-induced lung toxicity. The resident as well as the phagocytes infiltrating into the lungs, in response to the lung injury, may release pro-inflammatory cytokines and chemokines. The significant increase in the BALF levels of

MCP-1, MIP-2, and TNF-a, detected in the CNC exposed rats (Figure 8) were additional evidences for the induction of inflammation, in response to CNC exposure.

Bioinformatic analysis of the SDEGs identified, further supported the induction of inflammation, and provided important information with respect to the molecular mechanisms potentially underlying the CNC-induced lung inflammation and injury in the rats. Many of the significantly enriched and top-ranking IPA biological functions and canonical pathways detected were related to inflammation (Figures 9 and 10). A key event in the lung inflammation in response to injury by toxic particles such as CNC, is the recruitment of blood cells to the lungs (Yanamala et al. 2014; Sager et al. 2020). The movement of blood cells to the lungs is a complex process that involves processes such as activation and adhesion of blood cells, their movement through the circulatory system, and transmembrane migration from the blood vessels to the injury site(s) in the lungs. The transcripts for many cytokines and chemokines belonging to both the CXC and CCL groups, viz. *CCL2, CCL3, CCL4, CCL7, CCL17, CCL19, CCL22, CXCL1, CXCL2, CXCL4, CXCL6,* and *CXCL17* that serve as signaling molecules in the recruitment of inflammatory cells (Luster 1998; Lukacs et al. 1999; Gerard and Rollins 2001; Ono et al. 2003; Fulkerson et al. 2004) were significantly overexpressed in the CNC-exposed lungs suggesting their potential involvement in the recruitment of blood cells and the resulting lung inflammation induced by CNC. Macrophages undergo activation and differentiation prior to their recruitment in response to tissue injury and inflammation. The alternatively activated macrophages are characterized by the overexpression of genes such as *Arginase 1 (Arg1), Chitinase (Chia),* and *Resistin like alpha (Retnla)* (Loke et al. 2002; Raes et al. 2002; Gordon 2003; Nair et al. 2006). The significant overexpression of *Arg1, Chia,* and *Retnla* in the CNC exposed rat lungs (Supplemental Table 1) suggested their potential involvement in the activation of macrophages to engulf and eliminate the inhaled CNC particles from the lungs. The solute carrier 26a4 (Slc26a4) gene codes the protein, pendrin, which plays an active role in lung inflammation by facilitating the recruitment of PMNs (Nakao et al. 2008). The significant overexpression of the *Slc26a4* transcript (11.72-fold; Table 2) detected in the CNC exposed rat lungs was associated with a significant increase in the number of PMNs in the BAL (22.7-fold; Figure 5(D)). This suggested the potential involvement of the Slc26a4 gene in CNC-induced lung toxicity and inflammation like the role of this gene previously reported in crystalline silica-induced lung toxicity and inflammation (Sager 2019).

Activation of the complement system is a key event associated with the immune and inflammatory response to several stimuli including diseases and tissue injury by toxic particles (Pandya and Wilkes 2014; Husain et al. 2015). The complement system, functioning as a link between the innate and adaptive immunity, is regulated by complement proteins which are also synthesized by lung cells including alveolar type II epithelial cells (Strunk et al. 1988), bronchoalveolar epithelial cells (Varsano et al. 2000), and fibroblasts (Volanakis 1995). Additionally, AMs and PMNs can initiate the synthesis of complement proteins in response to inflammatory cytokines (Huber-Lang et al. 2002). The complement proteins in turn may function as chemoattractants for neutrophils, resulting in their infiltration into organs and induction of inflammation (Pandya and Wilkes 2014) such as that noticed in response to the lung injury caused by CNC exposure in rats. Activation of the complement system results in the formation of the membrane attack complex resulting in

cell lysis and tissue injury, a well-recognized consequence of complement system activation in the lungs (Sarma et al. 2006). The IPA canonical function, complement system, was significantly enriched in the CNC exposed rat lungs (Figure 10) and the transcripts for genes involved in complement response, viz. *Complement C1q A chain (C1QA), Complement C1q B chain (C1QB), Complement C1s (C1S), Complement 3 (C3), Complement 6 (C6), Complement factor B (CFB), Integrin subunit alpha M (ITGAM),* and *Integrin subunit alpha X (ITGAX),* were significantly overexpressed (Supplemental Table 1) suggesting the potential activation of the complement system and involvement in the lung response to CNC exposure in the rats.

Like the complement system, activation of acute phase response, is another key event involved in inflammatory response to tissue injury by toxic particles (Saber et al. 2014). Nanoparticles, compared with their larger counterparts, are more powerful inducers of acute phase response since the induction of acute phase response corresponds to the particle surface area (Saber et al. 2014). A significant enrichment in the acute phase response pathway (Figure 10) and overexpression of several acute phase response genes (Supplemental Tables 1 and 3) suggested the involvement of acute phase response in CNC-induced lung inflammation and toxicity. The transcript for the orosomucoid 1 gene that responds to tissue injury (Ligresti et al. 2012) and involved in inflammation (Alfadda et al. 2012) was 14.97-fold overexpressed in the CNC exposed rat lungs, compared with the control lungs (Table 2). Several other acute phase response genes were also significantly differentially expressed in the CNC-exposed rat lungs (Supplementary Tables 1 and 3). The serum level of serum amyloid A (SAA) protein is often considered a marker for the acute phase response (Sack 2018) and the transcript *Saal1 (Saa-like 1)* was 5.74-fold overexpressed in response to CNC exposure in the rat lungs. The significant differences in the expression of several genes involved in acute phase response in the CNC exposed rat lungs, compared with the controls, and the established role of acute phase response in inflammation may suggest the activation of acute phase response as a potential mechanism involved in the CNC-induced lung toxicity and inflammation.

The role of oxidative stress, resulting from excessive generation of reactive oxidants and/or the reduced detoxification of the oxidants generated in cells, in toxicity induced by particles (Sager et al. 2020), including that by nanoparticles (Manke et al. 2013), is well established. In agreement with the results of previous *in vitro* (Menas et al. 2017; Kisin et al. 2020) and *in vivo* (Yanamala et al. 2014; Farcas et al. 2016; Shvedova et al. 2016) studies, we found that the whole-body inhalation exposure of rats to CNC aerosol resulted in the generation of reactive oxidants in their lungs (Figure 7). This was accompanied by the significant enrichment in canonical pathways involved in oxidative stress, for example, NRF2-mediated oxidative stress response and production of nitric oxide and ROS in macrophages (Supplemental Table 3), and overexpression of genes involved either in the generation or detoxification of reactive oxidants (Supplemental Table 1). Reactive oxidants, like the pro-inflammatory molecules, are another class of molecules generated because of the interaction between the inhaled toxic particles, CNC for example, and the lung phagocytes which is regulated by the expression of several genes. The catalytic function of the protein encoded by the NADPH oxidase organizer 1 (NOXO1) gene results in the generation of superoxide anion (Katsuyama et al. 2012), which is subsequently dismutated

by superoxide dismutase (SOD) to generate hydrogen peroxide (H_2O_2). The *NOXO1* and *SOD2* transcripts were 2.98- and 2.42-fold, respectively, overexpressed in the CNC exposed lungs (Supplemental Table 1), thus favoring the generation of toxic H_2O_2 in the lungs. If not detoxified, H_2O_2 may result in toxicity and its interaction with free hemoglobin (Hb) is one such mechanism underlying the H_2O_2-induced toxicity (Schaer et al. 2013). Haptoglobin (HP), in addition to its role as an acute phase protein, may also function as an antioxidant by forming a complex with free Hb, thus preventing the generation of toxic, reactive oxygen species (Bertaggia et al. 2014). The significant overexpression of *HP* transcript detected (Supplemental Table 1) may, therefore, be considered as a modified response to prevent toxicity potentially resulting from oxidative stress in the lungs of the CNC exposed rats.

In addition to providing key information regarding the molecular mechanisms underlying the CNC-induced lung toxicity, the transcriptomic data obtained in this study suggested the potential for CNC exposure to result in cancer and extrapulmonary toxicity. The significant enrichment in the acute phase response pathway detected in the rats (Figure 10) may suggest the potential for CNC exposure to result in cardio-vascular diseases since activation of an acute phase response is both a risk factor (Lowe 2001) and a hallmark (Pai et al. 2004) for cardio-vascular diseases. Similarly, the significant enrichment in the functions and pathways related to cancer along with the physical properties of CNC such as its high aspect ratio and bio-persistence and the ability to induce inflammation and oxidative stress may be concerning from a human safety perspective. Currently there is no information whether CNC is bio-persistent in the lungs; however, the observation that CNC particles were not degraded in artificial alveolar macrophage phagolysosomal fluid over 9 months (Stefaniak et al. 2014) may suggest that CNC particles are likely to be persistent in the lungs. The bio-persistence of CNC in the lungs along with its ability to induce inflammation may result in chronic inflammation whose role in carcinogenesis is well established (Sollie et al. 2019). The suspected carcinogenic potential of CNC is further supported by its ability to transform cells *in vitro* to acquire neoplasitc properties (Kisin et al. 2020). In addition, the CNC-induced oxidant generation may also present a carcinogenic risk since oxidative stress is known to result in DNA damage – a major mechanism involved in carcinogenesis (Kurfurstova et al. 2016).

In conclusion, the data obtained in this study demonstrated lung toxicity in rats as an outcome to whole-body inhalation exposure to CNC and the involvement of inflammation and oxidant generation in the toxicity. The data, besides providing information regarding the molecular mechanisms underlying CNC-induced lung toxicity, suggested the potential risk for cardiovascular diseases and cancer in response to CNC exposure. However, further functional analysis of the significantly differentially expressed genes, for example, by transgenic techniques is required to validate the significance of the gene expression changes reported in this study. Based on the findings of the current study, future studies investigating CNC toxicity under realistic workplace exposure conditions of chronic, low level inhalation exposure are warranted. Such studies are required to determine the human safety of CNC – an emerging nanomaterial with many desirable properties and commercial and industrial applications.

Supplementary Material

Refer to Web version on PubMed Central for supplementary material.

Acknowledgements

The authors thank Howard Leonard and Aleks Stefaniak (NIOSH Morgantown, WV) for assistance with inhalation exposure of rats and for critical review of the manuscript, respectively.

Funding

Funding for this project was provided by Nanotechnology Research Center (NIOSH) [Project Numbers 921044E and 93909NA].

References

Alfadda AA, Fatma S, Chishti MA, Al-Naami MY, Elawad R, Mendoza CD, Jo H, Lee YS. 2012. Orosomucoid serum concentrations and fat depot-specific mRNA and protein expression in humans. Mol Cells 33(1):35–41. [PubMed: 22134720]

Ameen M, Musthapa M, Ahmad I, Ansari F, Baig M, Rahman Q. 2003. Alteration in cellular and biochemical markers of pulmonary toxicity in rat lung exposed to carpet dusts. Inhal Toxicol 15(11): 1119–1131. [PubMed: 12955617]

Andrews S 2010. FastQC: a quality control tool for high throughput sequence data http://www.bioinformatics.babraham.ac.uk/projects/fastqc.

Anjilvel S, Asgharian B. 1995. A multiple-path model of particle deposition in the rat lung. Toxicol Sci 28(1):41–50.

Bakand S, Hayes A, Dechsakulthorn F. 2012. Nanoparticles: a review of particle toxicology following inhalation exposure. Inhal Toxicol 24(2):125–135. [PubMed: 22260506]

Beck S, Bouchard J, Berry R. 2012. Dispersibility in water of dried nanocrystalline cellulose. Biomacromolecules 13(5):1486–1494. [PubMed: 22482888]

Bertaggia E, Scabia G, Dalise S, Lo Verso F, Santini F, Vitti P, Chisari C, Sandri M, Maffei M. 2014. Haptoglobin is required to prevent oxidative stress and muscle atrophy. PLoS One 9(6):e100745. [PubMed: 24959824]

Bolger AM, Lohse M, Usadel B. 2014. Trimmomatic: a flexible trimmer for Illumina sequence data. Bioinformatics 30(15):2114–2120. [PubMed: 24695404]

Butler C 1976. Lung surface area in various morphological forms of human emphysema. American Rev Resp Diseases 114:347–352.

Charreau H, Foresti ML, Vazquez A. 2013. Nanocellulose patents trends: a comprehensive review on patents on cellulose nanocrystals, microfibrillated and bacterial cellulose. Recent Pat Nanotechnol 7(1):56–80. [PubMed: 22747719]

Clift MJ, Foster EJ, Vanhecke D, Studer D, Wick P, Gehr P, Rothen-Rutishauser B, Weder C. 2011. Investigating the interaction of cellulose nanofibers derived from cotton with a sophisticated 3D human lung cell coculture. Biomacromolecules 12(10):3666–3673. [PubMed: 21846085]

Cullen RT, Searl A, Miller BG, Davis JM, Jones AD. 2000. Pulmonary and intraperitoneal inflammation induced by cellulose fibres. J Appl Toxicol 20(1):49–60. [PubMed: 10641016]

Ede JD, Ong KJ, Goergen M, Rudie A, Pomeroy-Carter CA, Shatkin JA. 2019. Risk analysis of cellulose nanomaterials by inhalation: current state of science. Nanomaterials (Basel). 9(3):337. [PubMed: 30832338]

Endes C, Schmid O, Kinnear C, Mueller S, Camarero-Espinosa S, Vanhecke D, Foster EJ, Petri-Fink A, Rothen-Rutishauser B, Weder C, et al. 2014. An in vitro testing strategy towards mimicking the inhalation of high aspect ratio nanoparticles. Part Fibre Toxicol 11(1):40. [PubMed: 25245637]

Farcas MT, Kisin ER, Menas AL, Gutkin DW, Star A, Reiner RS, Yanamala N, Savolainen K, Shvedova AA. 2016. Pulmonary exposure to cellulose nanocrystals caused deleterious effects

to reproductive system in male mice. J Toxicol Environ Health A 79(21): 984–997. [PubMed: 27558875]

Fulkerson PC, Zimmermann N, Hassman LM, Finkelman FD, Rothenberg ME. 2004. Pulmonary chemokine expression is coordinately regulated by STAT1, STAT6, and IFN-gamma. J Immunol 173(12):7565–7574. [PubMed: 15585884]

Gerard C, Rollins BJ. 2001. Chemokines and disease. Nat Immunol 2(2):108–115. [PubMed: 11175802]

Gordon S 2003. Alternative activation of macrophages. Nat Rev Immunol 3(1):23–35. [PubMed: 12511873]

Greenberg MI, Waksman J, Curtis J. 2007. Silicosis: a review. Dis Mon 53(8):394–416. [PubMed: 17976433]

Habibi Y, Lucia LA, Rojas OJ. 2010. Cellulose nanocrystals: chemistry, self-assembly, and applications. Chem Rev 110(6):3479–3500. [PubMed: 20201500]

Hubbe MA, Orlando JR, Lucian DL, Mohini S. 2008. Cellulose nanocomposites: a review. Bioresources 3:929–980.

Huber-Lang M, Younkin EM, Sarma JV, Riedemann N, McGuire SR, Lu KT, Kunkel R, Younger JG, Zetoune FS, Ward PA. 2002. Generation of C5a by phagocytic cells. Am J Pathol 161(5): 1849–1859. [PubMed: 12414531]

Husain M, Wu D, Saber AT, Decan N, Jacobsen NR, Williams A, Yauk CL, Wallin H, Vogel U, Halappanavar S. 2015. Intratracheally instilled titanium dioxide nanoparticles translocate to heart and liver and activate complement cascade in the heart of C57BL/6 mice. Nanotoxicology 9(8):1013–1022. [PubMed: 25993494]

Katsuyama M, Matsuno K, Yabe-Nishimura C. 2012. Physiological roles of NOX/NADPH oxidase, the superoxide-generating enzyme. J Clin Biochem Nutr 50(1):9–22. [PubMed: 22247596]

Kim D, Langmead B, Salzberg SL. 2015. HISAT: a fast spliced aligner with low memory requirements. Nat Methods 12(4):357–360. [PubMed: 25751142]

Kisin ER, Yanamala N, Rodin D, Menas A, Farcas M, Russo M, Guppi S, Khaliullin TO, Iavicoli I, Harper M, et al. 2020. Enhanced morphological transformation of human lung epithelial cells by continuous exposure to cellulose nanocrystals. Chemosphere 250:126170. [PubMed: 32114335]

Kurfurstova D, Bartkova J, Vrtel R, Mickova A, Burdova A, Majera D, Mistrik M, Kral M, Santer FR, Bouchal J, et al. 2016. DNA damage signalling barrier, oxidative stress and treatment-relevant DNA repair factor alterations during progression of human prostate cancer. Mol Oncol 10(6):879–894. [PubMed: 26987799]

Law CW, Alhamdoosh M, Su S, Dong X, Tian L, Smyth GK, Ritchie ME. 2016. RNA-seq analysis is easy as 1–2-3 with limma. F1000Res 5:1408.

Lee KY, Tammelin T, Schulfter K, Kiiskinen H, Samela J, Bismarck A. 2012. High performance cellulose nanocomposites: comparing the reinforcing ability of bacterial cellulose and nanofibrillated cellulose. ACS Appl Mater Interfaces 4(8):4078–4086. [PubMed: 22839594]

Li H, Handsaker B, Wysoker A, Fennell T, Ruan J, Homer N, Marth G, Abecasis G, Durbin R. 2009. The sequence alignment/map format and SAMtools. Bioinformatics 25(16):2078–2079. [PubMed: 19505943]

Ligresti G, Aplin AC, Dunn BE, Morishita A, Nicosia RF. 2012. The acute phase reactant orosomucoid-1 is a bimodal regulator of angiogenesis with time- and context-dependent inhibitory and stimulatory properties. PLoS One 7(8):e41387. [PubMed: 22916107]

Loke P, Nair MG, Parkinson J, Guiliano D, Blaxter M, Allen JE. 2002. IL-4 dependent alternatively-activated macrophages have a distinctive in vivo gene expression phenotype. BMC Immunol 3:7. [PubMed: 12098359]

Lowe GD. 2001. The relationship between infection, inflammation, and cardiovascular disease: an overview. Ann Periodontol 6(1):1–8.

Lukacs NW, Hogaboam C, Campbell E, Kunkel SL. 1999. Chemokines: function, regulation and alteration of inflammatory responses. Chem Immunol 72:102–120. [PubMed: 10550933]

Luster AD. 1998. Chemokines-chemotactic cytokines that mediate inflammation. N Engl J Med 338(7):436–445. [PubMed: 9459648]

Manke A, Wang L, Rojanasakul Y. 2013. Mechanisms of nanoparticle-induced oxidative stress and toxicity. Biomed Res Int 2013:942916. [PubMed: 24027766]

Mann PC, Vahle J, Keenan CM, Baker JF, Bradley AE, Goodman DG, Harada T, Herbert R, Kaufmann W, Kellner R, et al. 2012. International harmonization of toxicologic pathology nomenclature: an overview and review of basic principles. Toxicol Pathol 40(4 Suppl):7S–13S.

Mathew AP, Oksman K, Pierron D, Harmand MF. 2013. Biocompatible fibrous networks of cellulose nanofibres and collagen crosslinked using genipin: potential as artificial ligament/tendons. Macromol Biosci 13(3):289–298. [PubMed: 23225770]

McKinney W, Chen B, Schwegler-Berry D, Frazer DG. 2013. Computer-automated silica aerosol generator and animal inhalation exposure system. Inhal Toxicol 25(7):363–372. [PubMed: 23796015]

Menas AL, Yanamala N, Farcas MT, Russo M, Friend S, Fournier PM, Star A, Iavicoli I, Shurin GV, Vogel UB, et al. 2017. Fibrillar vs crystalline nanocellulose pulmonary epithelial cell responses: cytotoxicity or inflammation? Chemosphere 171:671–680. [PubMed: 28061425]

Moon RJ, Martini A, Nairn J, Simonsen J, Youngblood J. 2011. Cellulose nanomaterials review: structure, properties and nanocomposites. Chem Soc Rev 40(7):3941–3994. [PubMed: 21566801]

Morgan DL. 2006. NTP Toxicity Study Report on the atmospheric characterization, particle size, chemical composition, and workplace exposure assessment of cellulose insulation (CELLULOSEINS). Toxic Rep Ser 74:1–62, A1–C2.

Mroz RM, Schins RP, Li H, Jimenez LA, Drost EM, Holownia A, MacNee W, Donaldson K. 2008. Nanoparticle-driven DNA damage mimics irradiation-related carcinogenesis pathways. Eur Respir J 31(2):241–251. [PubMed: 18057054]

Nair MG, Guild KJ, Artis D. 2006. Novel effector molecules in type 2 inflammation: lessons drawn from helminth infection and allergy. J Immunol 177(3):1393–1399. [PubMed: 16849442]

Nakao I, Kanaji S, Ohta S, Matsushita H, Arima K, Yuyama N, Yamaya M, Nakayama K, Kubo H, Watanabe M, et al. 2008. Identification of pendrin as a common mediator for mucus production in bronchial asthma and chronic obstructive pulmonary disease. J Immunol 180(9):6262–6269. [PubMed: 18424749]

NIOSH. 2019. The National Institute for Occupational Safety and Health (NIOSH) pocket guide to chemical hazards – cellulose. The Centers for Disease Control and Prevention; [Accessed 2020 Nov 2]. https://www.cdc.gov/niosh/npg/npgd0110.html.

Ohashi T, Pinkerton K, Ikegami M, Jobe AH. 1994. Changes in alveolar surface area, surfactant protein A, and saturated phosphatidylcholine with postnatal rat lung growth. Pediatr Res 35(6):685–689. [PubMed: 7936819]

Ono SJ, Nakamura T, Miyazaki D, Ohbayashi M, Dawson M, Toda M. 2003. Chemokines: roles in leukocyte development, trafficking, and effector function. J Allergy Clin Immunol 111(6):1185–1199. [PubMed: 12789214]

Pai JK, Pischon T, Ma J, Manson JE, Hankinson SE, Joshipura K, Curhan GC, Rifai N, Cannuscio CC, Stampfer MJ, et al. 2004. Inflammatory markers and the risk of coronary heart disease in men and women. N Engl J Med 351(25):2599–2610. [PubMed: 15602020]

Pandya PH, Wilkes DS. 2014. Complement system in lung disease. Am J Respir Cell Mol Biol 51(4):467–473. [PubMed: 24901241]

Papageorgiou I, Brown C, Schins R, Singh S, Newson R, Davis S, Fisher J, Ingham E, Case CP. 2007. The effect of nano- and micronsized particles of cobalt-chromium alloy on human fibroblasts in vitro. Biomaterials 28(19):2946–2958. [PubMed: 17379299]

Park EJ, Khaliullin TO, Shurin MR, Kisin ER, Yanamala N, Fadeel B, Chang J, Shvedova AA. 2018. Fibrous nanocellulose, crystalline nanocellulose, carbon nanotubes, and crocidolite asbestos elicit disparate immune responses upon pharyngeal aspiration in mice. J Immunotoxicol 15(1):12–23. [PubMed: 29237319]

R Core Team. 2018. R: a language and environment for statistical computing Vienna, Austria: R Foundation for Statistical Computing. http://www.R-project.org/.

Raes G, De Baetselier P, Noel W, Beschin A, Brombacher F, Hassanzadeh Gh G, 2002. Differential expression of FIZZ1 and Ym1 in alternatively versus classically activated macrophages. J Leukoc Biol 71(4):597–602. [PubMed: 11927645]

Roberts JR, Anderson SE, Kan H, Krajnak K, Thompson JA, Kenyon A, Goldsmith WT, McKinney W, Frazer DG, Jackson M, et al. 2014. Evaluation of pulmonary and systemic toxicity of oil dispersant (COREXIT EC9500A(®)) following acute repeated inhalation exposure. Environ Health Insights 8(Suppl 1):63–74. [PubMed: 25861220]

Rol F, Sillard C, Bardet M, Yarava JR, Emsley L, Gablin C, Leonard D, Belgacem N, Bras J. 2020. Cellulose phosphorylation comparison and analysis of phosphorate position on cellulose fibers. Carbohydr Polym 229:115294. [PubMed: 31826473]

Saber AT, Jacobsen NR, Jackson P, Poulsen SS, Kyjovska ZO, Halappanavar S, Yauk CL, Wallin H, Vogel U. 2014. Particle-induced pulmonary acute phase response may be the causal link between particle inhalation and cardiovascular disease. Wiley Interdiscip Rev Nanomed Nanobiotechnol 6(6):517–531. [PubMed: 24920450]

Sack GH. Jr., 2018. Serum amyloid A – a review. Mol Med 24(1):46. [PubMed: 30165816]

Sager T 2019. Functional significance of the SLC26A4 gene in silica-induced pulmonary toxicity. Toxicol Suppl Toxicol Sci 168, Abstract No. 2017.

Sager T, Umbright C, Mustafa M, Yanamala N, Leonard H, McKinney W, Kashon M, Joseph P. 2020. Tobacco smoke exposure exacerbated crystalline silica-induced lung toxicity in rats. Toxicol Sci 178(2): 375–390. [PubMed: 32976597]

Sai T, Fujita K. 2020. A review of pulmonary toxicity studies of nanocellulose. Inhal Toxicol 32(6):231–239. [PubMed: 32460563]

Sarma VJ, Huber-Lang M, Ward PA. 2006. Complement in lung disease. Autoimmunity 39(5):387–394. [PubMed: 16923538]

Schaer CA, Deuel JW, Bittermann AG, Rubio IG, Schoedon G, Spahn DR, Wepf RA, Vallelian F, Schaer DJ. 2013. Mechanisms of haptoglobin protection against hemoglobin peroxidation triggered endothelial damage. Cell Death Differ 20(11):1569–1579. [PubMed: 23995229]

Seabra AB, Bernardes JS, Favaro WJ, Paula AJ, Duran N. 2018. Cellulose nanocrystals as carriers in medicine and their toxicities: a review. Carbohydr Polym 181:514–527. [PubMed: 29254002]

Sellamuthu R, Umbright C, Roberts JR, Chapman R, Young SH, Richardson D, Leonard H, McKinney W, Chen B, Frazer D, et al. 2011. Blood gene expression profiling detects silica exposure and toxicity. Toxicol Sci 122(2):253–264., [PubMed: 21602193]

Shackelford C, Long G, Wolf J, Okerberg C, Herbert R. 2002. Qualitative and quantitative analysis of nonneoplastic lesions in toxicology studies. Toxicol Pathol 30(1):93–96. [PubMed: 11890482]

Shatkin JA, Oberdorster G. 2016. Shvedova Comment on et al. (2016), “gender differences in murine pulmonary responses elicited by cellulose nanocrystals”. Part Fibre Toxicol 13(1):59. [PubMed: 27814761]

Shvedova AA, Kisin ER, Yanamala N, Farcas MT, Menas AL, Williams A, Fournier PM, Reynolds JS, Gutkin DW, Star A, et al. 2016. Gender differences in murine pulmonary responses elicited by cellulose nanocrystals. Part Fibre Toxicol 13(1):28. [PubMed: 27278671]

Siro L, Plackett M. 2010. Microfibrillated cellulose and new nanocomposite materials: a review. Cellulose 17(3):459–494.

Sollie S, Michaud DS, Sarker D, Karagiannis SN, Josephs DH, Hammar N, Santaolalla A, Walldius G, Garmo H, Holmberg L, et al. 2019. Chronic inflammation markers are associated with risk of pancreatic cancer in the Swedish AMORIS cohort study. BMC Cancer 19(1):858. [PubMed: 31464604]

Stefaniak AB, Seehra MS, Fix NR, Leonard SS. 2014. Lung biodurability and free radical production of cellulose nanomaterials. Inhal Toxicol 26(12):733–749. [PubMed: 25265049]

Strunk RC, Eidlen DM, Mason RJ. 1988. Pulmonary alveolar type II epithelial cells synthesize and secrete proteins of the classical and alternative complement pathways. J Clin Invest 81(5): 1419–1426. [PubMed: 2966814]

Varsano S, Kaminsky M, Kaiser M, Rashkovsky L. 2000. Generation of complement C3 and expression of cell membrane complement inhibitory proteins by human bronchial epithelium cell line. Thorax 55(5):364–369. [PubMed: 10770816]

Volanakis JE. 1995. Transcriptional regulation of complement genes. Annu Rev Immunol 13:277–305. [PubMed: 7612224]

Yanamala N, Farcas MT, Hatfield MK, Kisin ER, Kagan VE, Geraci CL, Shvedova AA. 2014. In vivo evaluation of the pulmonary toxicity of cellulose nanocrystals: a renewable and sustainable nanomaterial of the future. ACS Sustain Chem Eng 2(7):1691–1698. [PubMed: 26753107]

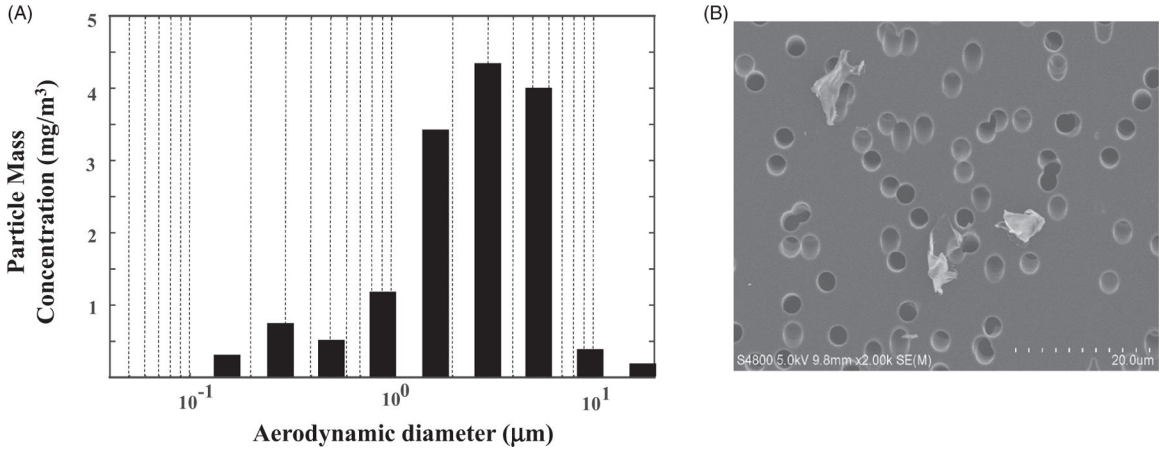

Figure 1.

Size distribution and morphology of CNC particles in the aerosol generated for rat whole-body inhalation exposure. An aerosol containing CNC particles was generated as described in the Materials and Methods section. The aerosol was analyzed for particle size distribution using a MOUDI (A) and for particle size using an electron microscope (B) as described in the Materials and Methods section.

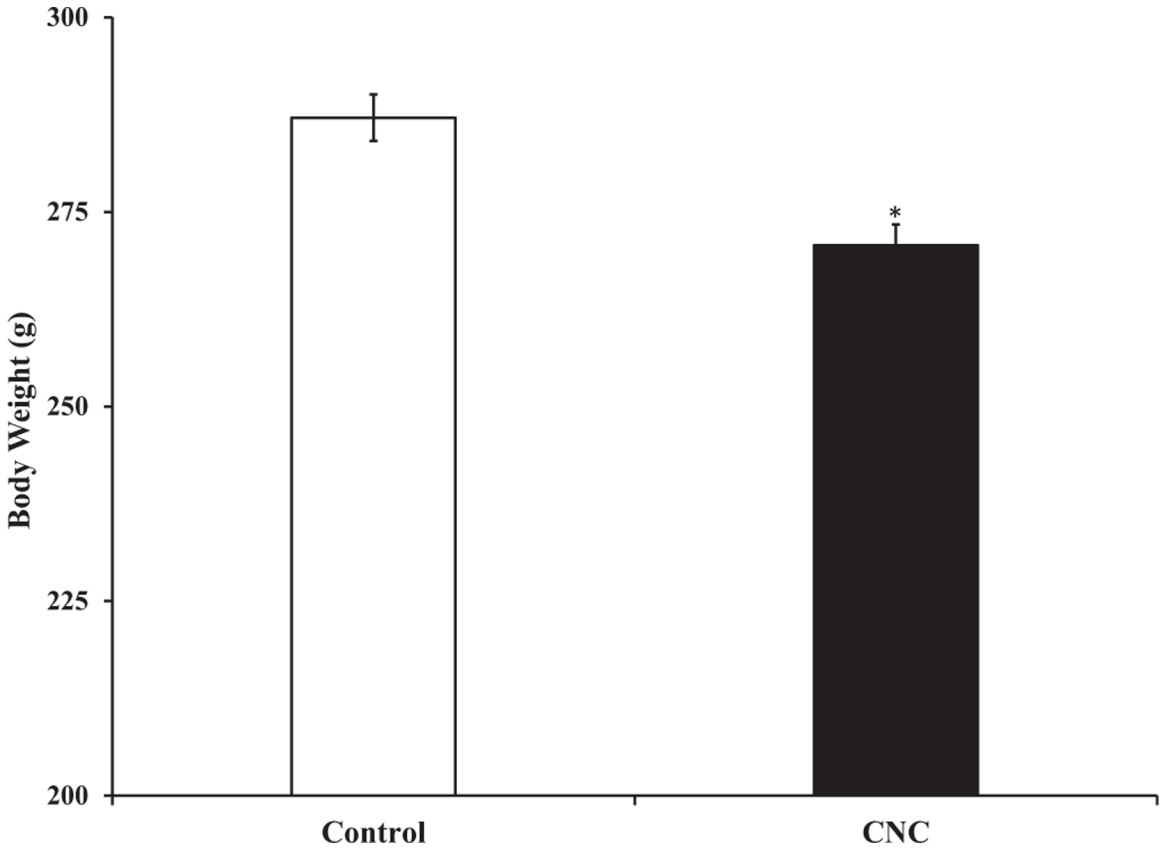

Figure 2.

Body weights of rats. Body weights (g) of the air and CNC exposed rats were determined at the end of the study immediately before euthanasia. Body weights (g) are represented as mean ± S.E. (n=12). *p<0.05.

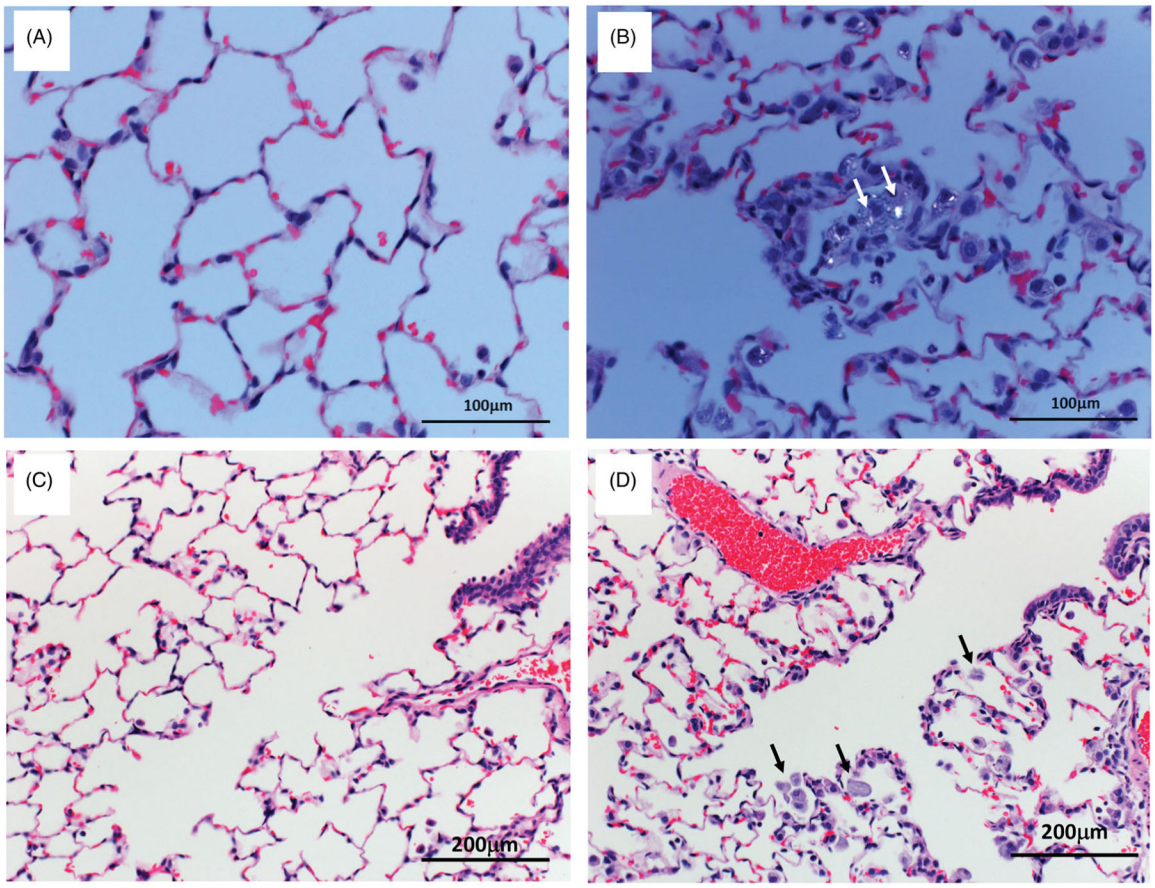

Figure 3.

Photomicrographs of lung sections from the control and CNC exposed rats. Rats were exposed to air or an aerosol containing CNC and the lung sections were stained with hematoxylin and eosin and analyzed for histological changes as described in the Materials and Methods section. Polarizing light microscopy demonstrated numerous birefringent crystals (white dots) within an accumulation of alveolar macrophages (white arrows) (B). Increased numbers of alveolar macrophages (black arrows) are present in the alveolar duct of a rat exposed to CNC (D). Panels A and C show normal pulmonary architecture in an air-exposed control animal. Panels A and B magnification is 400x and Panels C and D magnification is 200x.

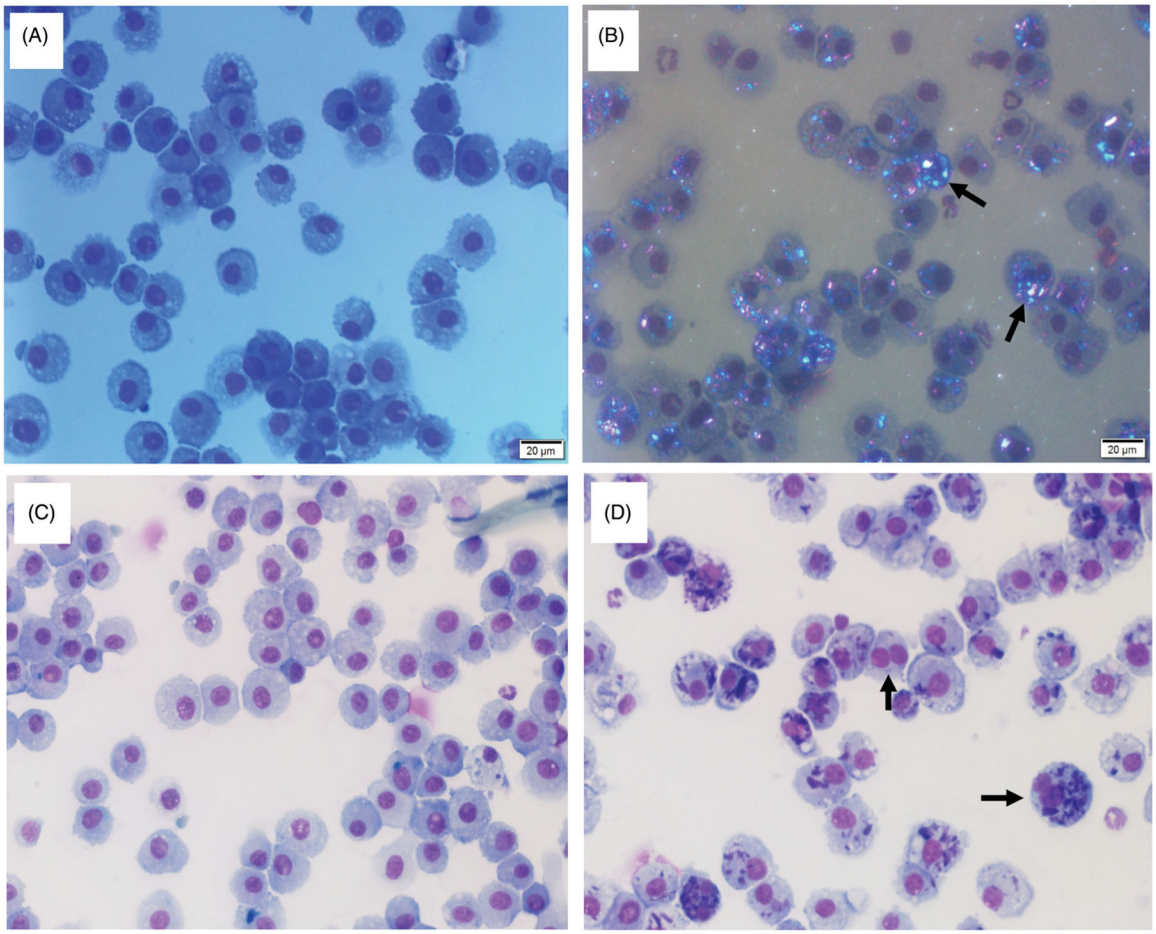

Figure 4.

Bronchoalveolar lavage cells showing binucleated AMs and AMs containing CNC particles. Rats were exposed to air (control) or an aerosol containing CNC and lung lavage following euthanasia was conducted and cytospin slides were prepared as described in the Materials and Methods section. The cytospin slides were stained with a Leukostat stain and observed under a microscope. A and B – micrographs of cells observed under polarizing light showing the presence of birefringent CNC particles engulfed by AMs (arrows) in the CNC exposed lung cells (B). C and D – micrographs of cells observed under a light microscope showing binucleated AMs (arrows) in the CNC exposed lung cells (D). AMs with more than two nuclei were not detected.

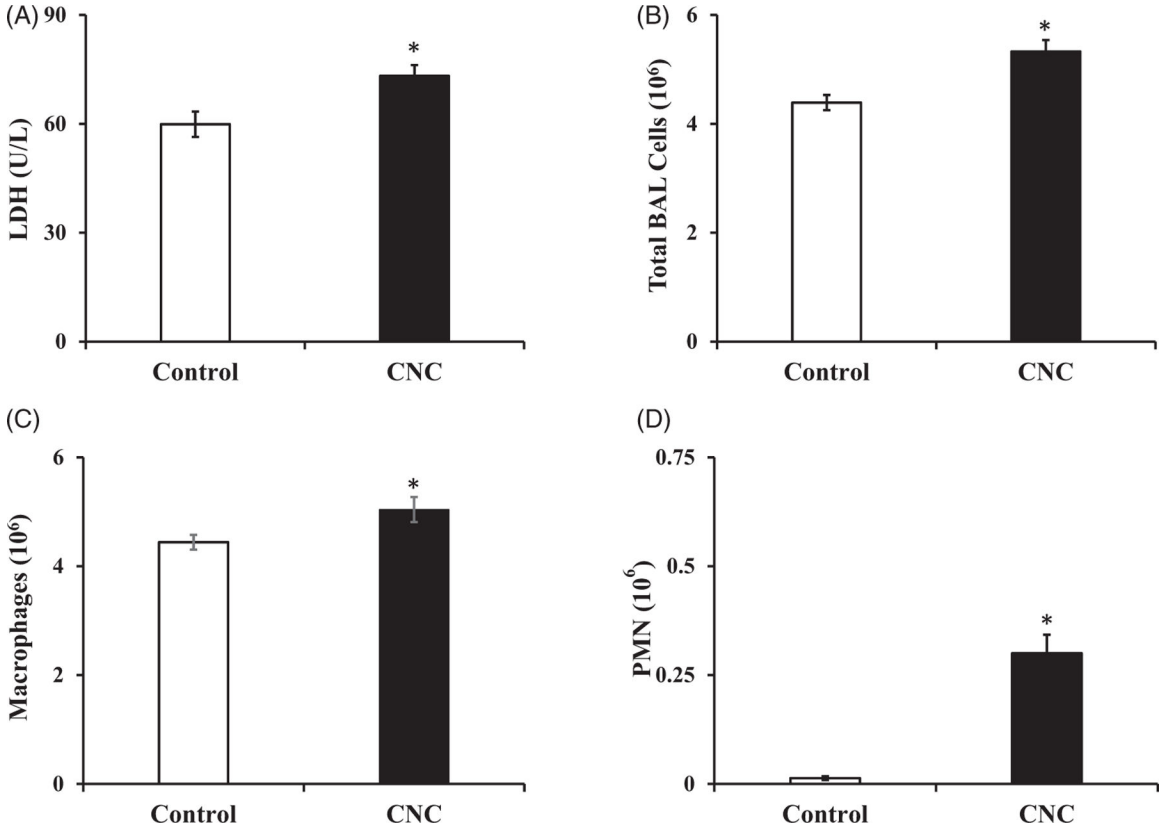

Figure 5.

Bronchoalveolar lavage parameters of lung response in the control and CNC exposed rats. Groups of rats were exposed to air or CNC and lung lavage was performed following euthanasia as described in the Materials and Methods section. Bronchoalveolar lavage (BAL) parameters of lung response, viz. LDH activity (A), total BAL cells (B), AMs (C), and PMNs (D) were determined as described in the Materials and Methods section. Data represent mean ± S.E. [(n=11 (Total BAL cells, Macrophages, and PMN) or 12 (LDH)]. *p<0.05.

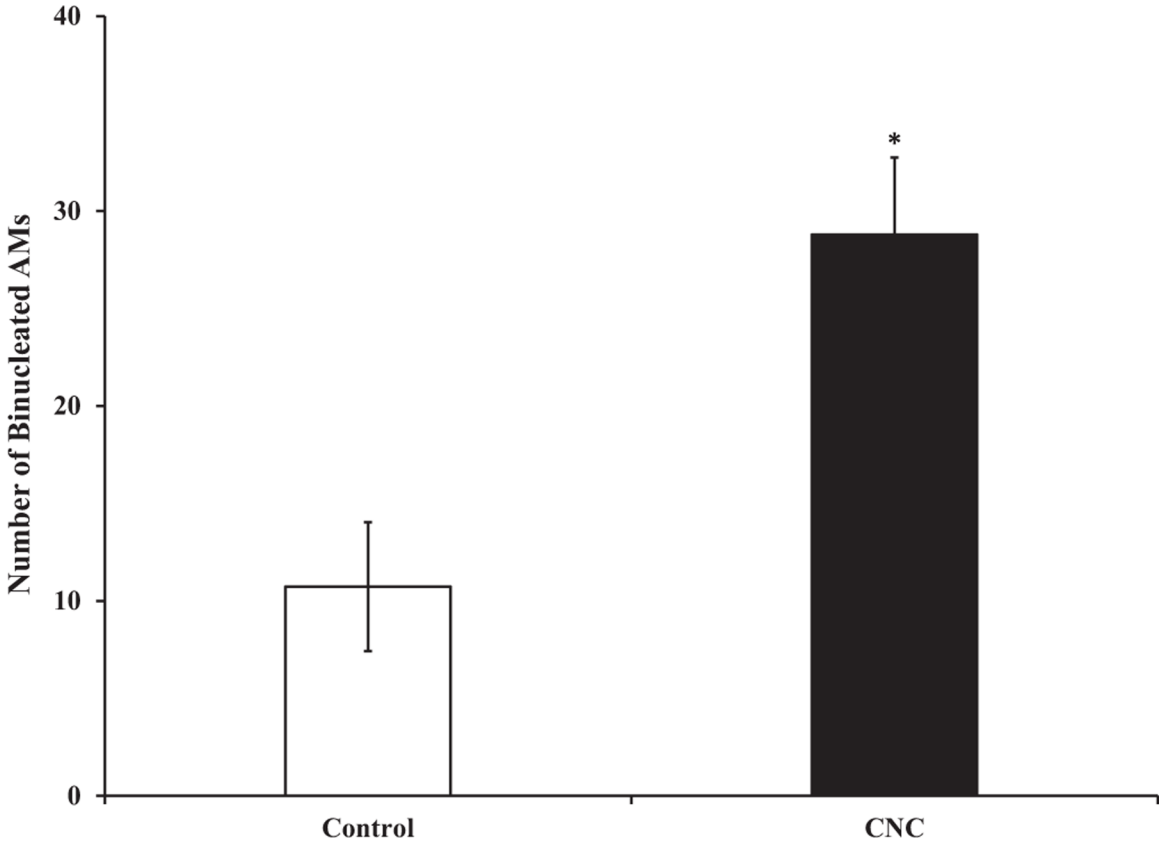

Figure 6.

Binucleated AMs in the BAL cells. Rats were exposed to air (control) or an aerosol containing CNC and lung lavage following euthanasia was conducted and cytospin slides were prepared and stained with a Leukostat stain as described in the Materials and Methods section. The cytospin slides were observed under a light microscope and the number of binucleated cells were recorded. Data represent mean ± S.E. (n=6). *p<0.05.

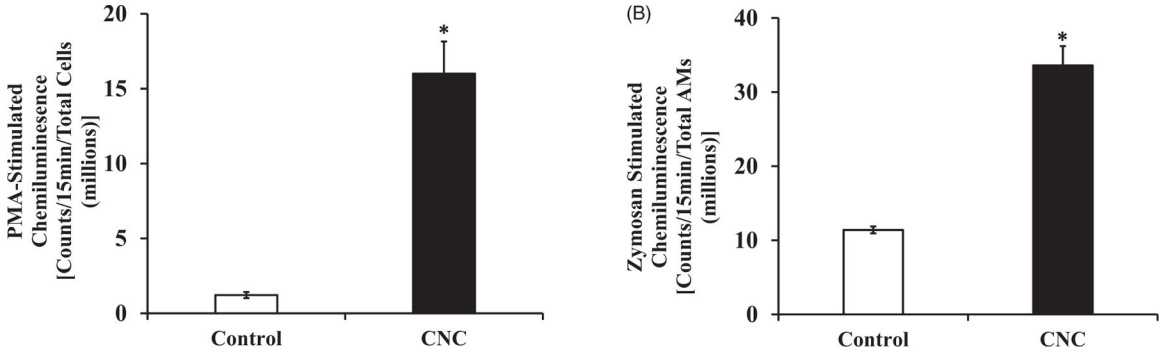

Figure 7.

Oxidant generation by BAL phagocytes in the control and CNC exposed rats. Groups of rats were exposed to air (control) or an aerosol containing CNC and lung lavage following euthanasia was conducted. The oxidants generated by the phagocytes present in the BAL cells were determined as described in the Materials and Methods section. Data represent mean ± S.E. (n=12). *p<0.05.

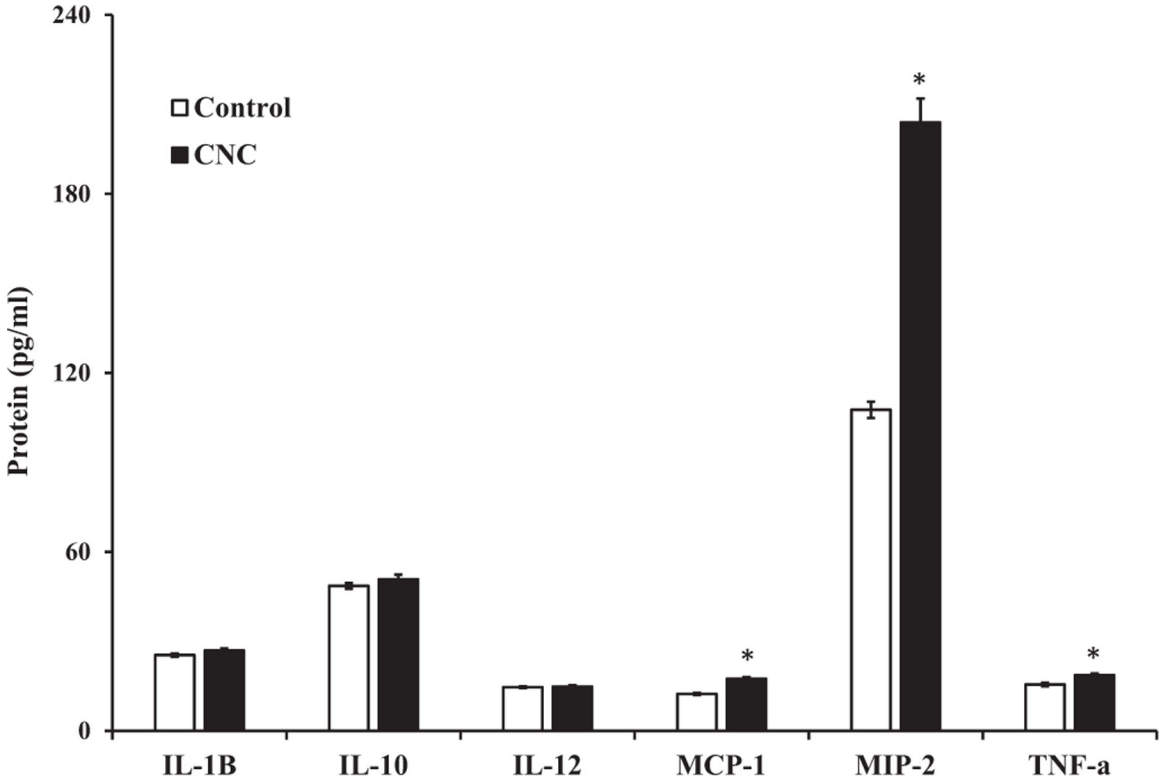

Figure 8.

Cytokines in the BALF of the control and CNC exposed rats. Groups of rats were exposed to air (control) or CNC as described in the Materials and Methods section. The BAL collected following euthanasia of the rats were processed to obtain cell-free BALF and analyzed for the various cytokines by ELISA as described in the Materials and Methods section. Data represent mean ± S.E. (n=12). *p<0.05.

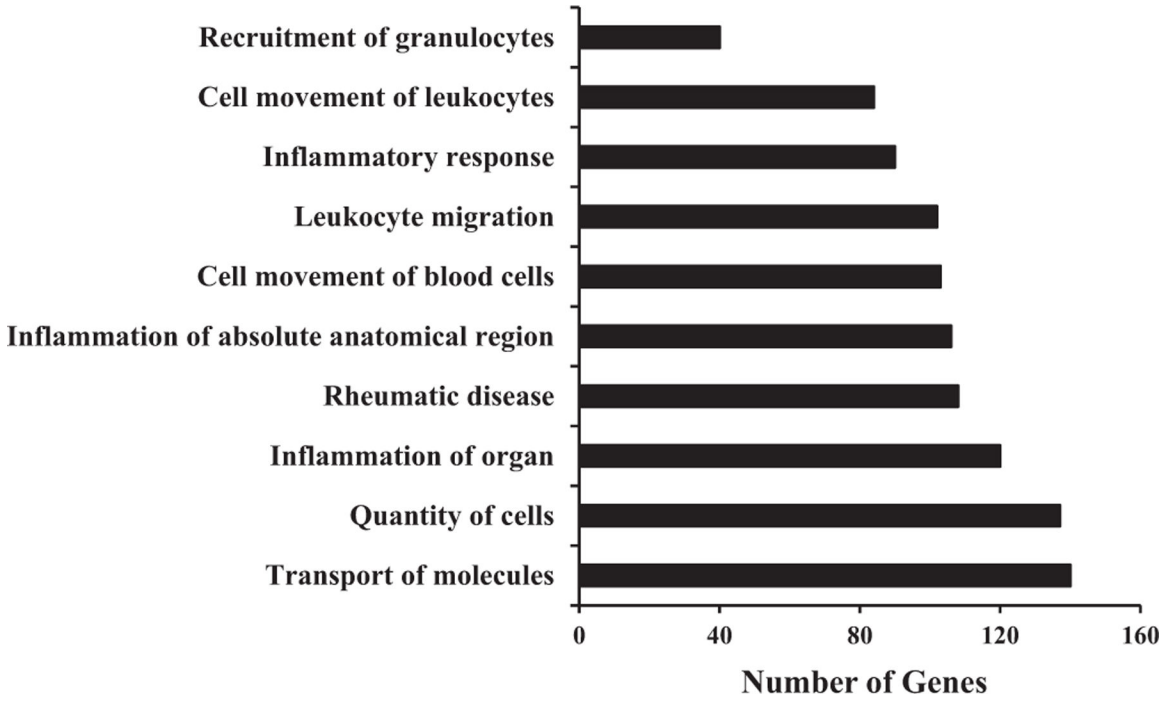

Figure 9.

IPA Biological functions and disease categories enriched in the lungs of the CNC exposed rats. Genes exhibiting significant differential expression (FC > 1.5 and adjusted *p* value <0.05) in the lungs of the CNC exposed rats, compared with the controls, were identified by NGS analysis as described in the Materials and Methods section. Enrichment analysis of the significantly differentially expressed genes was performed using the IPA program. Ten of the top ranking enriched biological function and disease categories are presented. A complete list of the enriched biological functions and diseases categories and the genes involved in each category are presented in Supplemental Table 2.

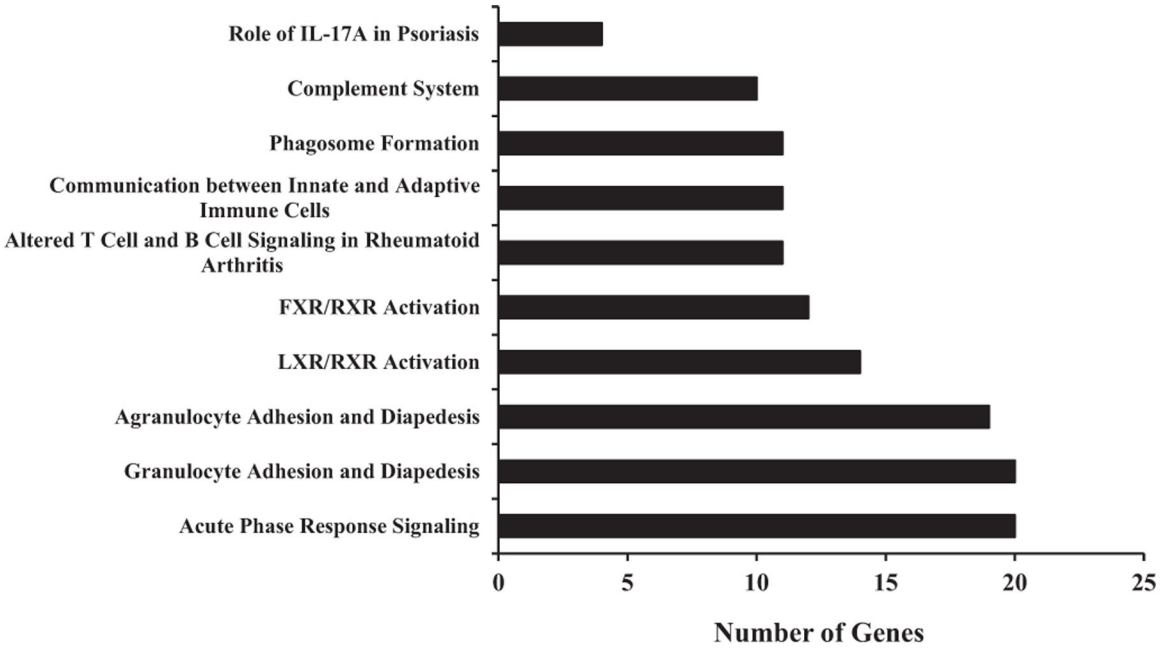

Figure 10.

IPA Canonical pathways enriched in the lungs of the CNC exposed rats. Genes exhibiting significant differential expression (FC > 1.5 and adjusted *p* value <0.05) in the lungs of the CNC exposed rats, compared with the control lungs, were identified by NGS analysis as described in the Materials and Methods section. Enrichment analysis of the significantly differentially expressed genes was performed using the IPA program. Ten of the top ranking enriched canonical pathways are presented. A complete list of the enriched canonical pathways and the genes involved in each pathway are presented in Supplemental Table 3.

Table 1.

Results of the hematology parameters determined in the rats.

	Exposure	
Parameter	**Air**	**CNC**
Red Blood Cells (RBC) (M/ml)	8.97 ± 0.06	9.2 ± 0.04 *
RDW-SD	30.73 ± 0.34	29.35 ± 0.02 *
Reticulocytes (RET) (K/ml)	285.65 ± 6.62	229.25 ± 5.80 *
Reticulocytes (RET) (%)	3.19 ± 0.08	2.49 ± 0.06 *
P-LCR (%)	9.16 ± 0.29	8.35 ± 0.03 *
Neutrophils (%)	20.92 ± 0.65	23.7 ± 0.86 *

None of the other hematology parameters analyzed showed a statistically significant difference between the control and CNC exposed groups and the results are not presented. Data represent mean ± S.E. (n=11).

* p<0.05

Table 2.

Top 20 up-regulated genes in the rat lungs in response to CNC exposure.

Transcript	Fold change	Adjusted *p* value
Defensin beta 5 (Defb5)	17.21	2.40E-05
Membrane-spanning 4-domains, subfamily A, member 6B-like (Ms4a6bl)	15.57	3.16E-03
Orosomucoid 1 (Orm1)	14.97	5.88E-07
Solute carrier family 26 member 4 (Slc26A4)	11.72	1.45E-06
Tetraspanin 10 (Tspan10)	10.32	5.26E-06
Protease, serine, 30 (Prss30)	9.11	1.17E-03
CD177 molecule (CD177)	7.84	1.30E-06
Inter-alpha trypsin inhibitor, heavy chain 1 (Itih1)	7.10	4.50E-06
Resistin like alpha (Retnla)	6.82	3.63E-06
Mab-21 like 3 (Mab21l3)	6.70	1.51E-04
Lymphocyte antigen 6 complex, locus A-like (Ly6al)	6.36	4.29E-05
Lipocalin 2 (LCN2)	6.06	9.20E-07
C-X-C motif chemokine ligand 6 (Cxcl6)	5.81	7.98E-06
Serum amyloid A-like (saal1)	5.74	1.30E-06
Matrix metallopeptidase 12 (MMP12)	5.58	1.89E-05
Rhomboid like 2 (Rhbdl2)	5.51	4.90E-06
Transmembrane protein 45 b (Tmem45b)	5.42	1.75E-05
C-C motif chemokine ligand 22 (Ccl22)	5.20	6.95E-05
BPI fold containing family B, member 1 (Bpifb1)	5.16	1.89E-03
ATPase H + transporting V0 subunit D2 (Atp6v0d2)	4.58	3.93E-06

A complete list of the 531 SDEGs and their fold changes in expression and adjusted p values are presented in Supplemental Table 1.

Table 3.

Top 20 down-regulated genes in rat lungs in response to CNC exposure.

Transcript	Fold change	Adjusted *p* value
Delta like non-canonical notch ligand 1 (Dlk1)	−20.03	6.53E-05
Similar to GTL2, imprinted maternally expressed, untranslated (RGD1566401)	−9.03	1.92E-04
Ribosomal protein L10-like (Rpl10l)	−4.39	6.39E-03
Potassium calcium-activated channel subfamily M regulatory beta subunit 2 (Kcnmb2)	−3.10	8.63E-06
Similar to hypothetical protein (RGD1566226)	−2.81	6.37E-03
Coiled-coil domain containing 152 (Ccdc152)	−2.48	1.28E-02
Somatomedin B and thrombospondin, type 1 domain containing (Sbspon)	−2.41	4.11E-02
Megalencephalic leukoencephalopathy with subcortical cysts 1 (Mlc1)	−2.35	4.75E-04
Natriuretic peptide receptor 3 (Npr3)	−2.34	3.21E-04
Arachidonate 15-lipoxygenase (Alox15)	−2.33	7.78E-05
C-C motif chemokine ligand 24 (Ccl24)	−2.08	3.35E-03
Elastin (Eln)	−2.07	2.62E-06
Spondin 2 (Spon2)	−2.06	5.37E-06
Synaptonemal complex protein 2 (Sycp2)	−2.01	1.29E-03
Calcineurin-like EF hand protein 2 (Chp2)	−1.95	5.17E-04
Aryl hydrocarbon receptor nuclear translocator-like (Arntl1)	−1.94	1.16E-04
Arylsulfatase family, member I (Arsi)	−1.93	8.07E-05
Potassium channel tetramerization domain containing 8 (Kctd8)	−1.92	6.57E-04
Dual specificity phosphatase 14-like 1 (Dusp14l1)	−1.91	1.33E-02
Similar to ankyrin repeat domain 26(LOC685215)	−1.91	1.37E-02

A complete list of the 531 SDEGs and their fold changes in expression and adjusted p values are presented in Supplemental Table 1.